Removal of bisphenol A from acidic sulfate medium and urban wastewater using persulfate activated with electroregenerated Fe^{2+}

Alexsandro Jhones dos Santos, Ignasi Sirés, Enric Brillas*

Laboratori d'Electroquímica dels Materials i del Medi Ambient, Departament de Química Física, Facultat de Química, Universitat de Barcelona, Martí i Franquès 1-11, 08028 Barcelona, Spain

**Corresponding author's* e-*mail address*: brillas@ub.edu (E. Brillas)

Abstract

Model solutions of bisphenol A (BPA) in 0.050 M Na_2SO_4 at pH 3.0 have been treated by the electro/Fe^{2+}/persulfate process. The activation of 5.0 mM persulfate with 0.20 mM Fe^{2+} yielded a mixture of sulfate radical anion ($SO_4^{\bullet-}$) and $^{\bullet}OH$, although quenching tests revealed the prevalence of the former species as the main oxidizing agent. In trials run in an IrO_2/carbon-felt cell, 98.4% degradation was achieved alongside 61.8% mineralization. The energy consumption was 253.9 kWh (kg TOC)$^{-1}$, becoming more cost-effective as compared to cells with boron-doped diamond and Pt anodes. Carbon felt outperformed stainless steel as cathode because of the faster Fe^{2+} regeneration. All BPA concentration decays agreed with a pseudo-fist-order kinetics. The effect of persulfate, Fe^{2+} and BPA concentrations as well as of the applied current on the degradation process was assessed. Two dehydroxylated and three hydroxylated monobenzenic by-products appeared upon $SO_4^{\bullet-}$ and $^{\bullet}OH$ attack, respectively. The analogous treatment of BPA spiked into urban wastewater yielded a faster degradation and mineralization due to the co-generation of HClO and the larger $^{\bullet}OH$ production as $SO_4^{\bullet-}$ reacted with Cl^-.

Keywords: Carbon-felt cathode; Emerging contaminant; Hydroxyl radical; Persulfate; Sulfate radical anion; Water treatment

1. Introduction

Bisphenol A (BPA) is a well-known endocrine disruptor with severe impact on human fertility (Rochester, 2013; Matuszczak et al., 2019). It is present in a large variety of industrial and personal care products such as plastics, resins, lotions, cleaners, body creams and shampoos (Bhatnagar and Anastopoulos, 2017). BPA is highly soluble in water (300 mg L^{-1} at 25 ºC, Careghini et al., 2015) and, consequently, it has been detected in natural water and wastewater at concentrations between 1.3 and 370 μg L^{-1}, in landfill leachates up to 17 mg L^{-1} and in sewage sludges, sediments and biosolids up to 95 mg kg^{-1} (Corrales et al., 2015; Petrie et al., 2015). The development of technologies for the destruction of BPA in aqueous effluents is then mandatory, aiming to avoid its hazardous effects on living beings.

Physicochemical methods like adsorption (Bhatnagar and Anastopoulos, 2017) and chemical ones including ozonation (Umar et al., 2013), photo-Fenton (Molkenthin et al., 2013) and, more recently, activated persulfate ($S_2O_8^{2-}$, PS) have been applied to remove BPA from water. PS activation consists in its conversion into sulfate radical anion ($SO_4^{\bullet-}$). Ozone (Yang et al., 2016), H_2O_2/Fe^{2+} (Khandarkhaeva et al., 2019), H_2O_2/Fe_3O_4 (Xu et al., 2019), H_2O_2/zero valent iron (Girit et al., 2015; Wu et al., 2020), Fe_3O_4-α-MnO_2 (Dong et al., 2019) and Fe^{2+} (Jiang et al., 2013; Kang et al., 2018) behave as effective activators. Reaction (1) accounts for the production of $SO_4^{\bullet-}$ from PS and Fe^{2+}. This radical can be partially deactivated by Fe^{2+} via reaction (2) (Yang, 2015; Matzek and Carter, 2016). Reaction (3) between PS and an organic molecule R also originates $SO_4^{\bullet-}$ (Matzek and Carter, 2016). A remarkable feature of $SO_4^{\bullet-}$ is its ability to generate $^{\bullet}OH$, either via reaction (4) at pH < 7 or reaction (5) in alkaline medium (Devi et al., 2016; Matzek and Carter, 2016). It has been established that the predominant species is $SO_4^{\bullet-}$ at pH < 7 and $^{\bullet}OH$ at pH 12, whereas none of them prevails at pH 9 (Romero

et al., 2010; Akbari et al., 2016). Moreover, $SO_4^{\bullet-}$ can dimerize to form $S_2O_8^{2-}$ according to parasitic reaction (6).

$$S_2O_8^{2-} + Fe^{2+} \rightarrow Fe^{3+} + SO_4^{\bullet-} + SO_4^{2-} \quad (1)$$

$$SO_4^{\bullet-} + Fe^{2+} \rightarrow SO_4^{2-} + Fe^{3+} \quad (2)$$

$$S_2O_8^{2-} + R \rightarrow 2SO_4^{\bullet-} + R^{\bullet} \quad (3)$$

$$SO_4^{\bullet-} + H_2O \rightarrow SO_4^{2-\cdot} + {}^{\bullet}OH + H^{+} \quad (4)$$

$$SO_4^{\bullet-} + OH^{-} \rightarrow SO_4^{2-\cdot} + {}^{\bullet}OH \quad (5)$$

$$2SO_4^{\bullet-} \rightarrow S_2O_8^{2-} \quad (6)$$

$SO_4^{\bullet-}$ is a strong oxidant with a standard reduction potential (E^{o}) of 2.44 V|SHE, slightly lower than E^{o} = 2.73 V|SHE shown by $^{\bullet}OH$. However, this is counterbalanced by its much longer lifetime, making feasible its fast reaction with aromatic compounds (Armstrong et al., 2015; Wojnárovits and Takács, 2019). The removal of BPA from aqueous solutions has been studied by electrochemical advanced oxidation processes (EAOPs) like electrochemical oxidation (EO), electro-Fenton (EF) an photoelectro-Fenton (PEF). These EAOPs involve the generation of $^{\bullet}OH$ and their immediate action on organic pollutants (Martínez-Huitle et al., 2015; Moreira et al., 2017; Lanzalaco et al., 2018; Brillas, 2020; dos Santos et al., 2020). In EO, the effectiveness of different anodes like boron-doped diamond (BDD) (Murugananthan et al., 2008; Cui et al., 2009), B-doped graphene (Wu et al., 2019), doped SnO_2 (Cui et al., 2009), Pt (Li et al., 2016) and dimensionally stable anodes (DSA) (Cui et al., 2009) has been investigated. The quickest BPA removal was achieved with non-active BDD anodes because of the higher quantity of physisorbed $^{\bullet}OH$ produced from water discharge via reaction (7) (Panizza and Cerisola, 2009; Oturan and Aaron, 2014; Galia et al., 2016). Thus, Murugananthan et al. (2008) found that 20 mg L^{-1} BPA in a 0.10 M Na_2SO_4 solution at pH 6 treated by EO with

BDD were completely mineralized after 12 h at a current density of 35.7 mA cm^{-2}, yielding phenol, hydroquinone and *p*-benzoquinone as by-products.

$$M + H_2O \rightarrow M(^{\bullet}OH) + H^+ + e^- \quad (7)$$

EF process also ensured a large mineralization of BPA solutions, owing to the contribution of homogeneous $^{\bullet}OH$ formed from Fenton's reaction between added Fe^{2+} and electrogenerated H_2O_2 (Gözmen et al., 2003; dos Santos et al., 2016, 2018a; Chmayssem et al., 2017). A faster degradation was reported by Burgos-Castillo et al. (2018) when solutions of 150 mL containing 0.556 mM BPA in 0.050 M Na_2SO_4 and 0.50 mM Fe^{2+} at pH 3.0 were treated by PEF with a BDD anode, a carbon-PTFE air-diffusion cathode and a 6 W UVA lamp at 33.3 mA cm^{-2} for 360 min.

More recently, Ding et al. (2020) enhanced the EO treatment of BPA in sulfate medium by employing a divided cell to activate PS in the anodic compartment. For solutions with 5 μM BPA, 0.030 M Na_2SO_4 and 1 mM PS treated at 5 mA cm^{-2} for 30 min, they reported a similar degradation near 50% regardless of the anode material. The production of oxidants ($SO_4^{\bullet-}$ and $^{\bullet}OH$) was thus analogous using BDD or DSA. Under these conditions, $SO_4^{\bullet-}$ can be formed via: (i) reaction (8), as PS is activated by $^{\bullet}OH$ formed from reaction (7), and (ii) SO_4^{2-} oxidation at the anode from reaction (9) (Matzek and Carter, 2016; Luo et al., 2017; Liu et al., 2018).

$$S_2O_8^{2-} + {}^{\bullet}OH \rightarrow HSO_4^- + SO_4^{\bullet-} + ½O_2 \quad (8)$$

$$SO_4^{2-} \rightarrow SO_4^{\bullet-} + e^- \quad (9)$$

Another interesting approach within the electrochemical routes, which has been only examined by few authors, consists in the simultaneous promotion of the cathodic Fe^{2+} electrogeneration in an undivided cell. In such system, $SO_4^{\bullet-}$ can be produced by direct reduction of PS at the cathode via reaction (10), whereas Fe^{2+} is regenerated as Fe^{3+} is reduced via reaction (11). This accelerates the $SO_4^{\bullet-}$ generation from reaction (1), although Fe^{2+} can be

partly oxidized to Fe^{3+}at the anode from reaction (12) (Wu et al., 2012; Devi et al., 2016; Matzek and Carter, 2016). This approach has been tested to treat acidic BPA solutions, obtaining an effective degradation but poor mineralization using DSA/stainless steel (SS) (Lin et al., 2013) and graphite/graphite (Yang, 2015; Akbari et al., 2016) cells. Worth noting, 3D cathodes, which have a much larger electroactive surface area, have never been employed to this purpose. This type of material could largely improve the kinetics of reaction (11), eventually upgrading the direct formation of $SO_4^{\bullet-}$ from reaction (1) and the indirect generation of homogeneous $^{\bullet}OH$ from reaction (4). Among such 3D cathodes, carbon felt seems suitable due to its low cost and large ability to regenerate Fe^{2+} in acidic medium (Sirés et al., 2007; El-Ghenymy et al. 2014).

$$S_2O_8^{2-} + e^- \rightarrow SO_4^{2-\cdot} + SO_4^{\bullet-} \quad (10)$$

$$Fe^{3+} + e^- \rightarrow Fe^{2+} \quad (11)$$

$$Fe^{2+} \rightarrow Fe^{3+} + e^- \quad (12)$$

The aim of this work is to study of the degradation and mineralization of BPA in acidic sulfate medium, in the presence of PS and Fe^{2+}, upon electrolysis in an undivided cell equipped with a DSA (Ti/IrO_2) anode and a carbon-felt cathode, so-called electro/Fe^{2+}/PS process. Comparative assays were made to show the benefits of combining PS and Fe^{2+} with the 3D cathode. The performance of cells equipped with a BDD or Pt anode and an SS cathode was analyzed as well. The effect of the concentrations (BPA, PS and Fe^{2+}) and applied current (*I*), on the performance of the process was evaluated. The main by-products formed were detected by gas chromatography-mass spectrometry (GC-MS). Finally, the viability of the electrochemical process was corroborated by treating BPA in urban wastewater.

2. Materials and methods

2.1. Chemicals and aqueous matrices

Commercial BPA ($C_{15}H_{16}O_2$, M = 228.29 g mol^{-1}, > 99% purity) was supplied by Sigma-Aldrich. Methanol and *tert*-butanol used as radical scavengers were of analytical grade, purchased from Sigma-Aldrich. Na_2SO_4, $Na_2S_2O_8$ and $FeSO_4$•$7H_2O$ were of analytical grade, supplied by Prolabo, Sigma-Aldrich and Fluka, respectively. The initial pH was adjusted to 3.0 with H_2SO_4 (98% purity) purchased from Merck and analytical grade NaOH purchased from Panreac. Analytical solutions were prepared with ultrapure water (Millipore Milli-Q, resistivity >18.2 MΩ cm). All the other chemicals used for analysis were of analytical or HPLC grade provided by Merck and Panreac.

To carry out the electrolytic assays, BPA was spiked into aqueous matrices with the following composition:

(i) Ultrapure water containing 0.050 M Na_2SO_4 at pH 3.0, showing a specific conductivity of 7.1 mS cm^{-1}.

(ii) Urban wastewater obtained from the secondary effluent of a wastewater treatment plant, with pH 7.3, conductivity of 1.29 mS cm^{-1} and total organic carbon (TOC) of 11.8 mg L^{-1} (detailed composition reported by Ye et al. (2020)).

2.2. Electrolytic treatments

The electrolytic experiments were made in an undivided glass cell (6 cm diameter and 250 mL capacity), which was able to keep the solution temperature at 35 ºC thanks to water recirculated through an external water circuit. All the assays were made with a solution volume of 130 mL and magnetic stirring. The anode of 3 cm^2 was either a BDD thin film onto Si purchased from NeoCoat, a Pt foil (99.99% purity) provided by SEMPSA or an IrO_2-based (DSA-O_2) plate purchased from NMT Electrodes.The piece was centered in the cell, surrounded by a 30 cm^2 carbon felt cathode supplied by Carbon-Lorraine. In some assays, a 3 cm^2 SS (AISI 304) sheet was used as the cathode. The distance between the anode and cathode was always 1 cm. Note that the trials were made in the absence of air sparging, aiming to limit the H_2O_2

electrogeneration. An Amel 2049 potentiostat-galvanostat was utilized to supply a constant *I* to the electrodes, whereas the cell voltage was continuously monitored with a digital multimeter. Before the tests, all the anodes and cathodes were cleaned by means of a polarization in a 0.050 M Na_2SO_4 solution at pH 3.0 and 200 mA for 360 min.

2.3. Analytical procedures

The instruments utilized for the pH and conductivity measurements and the determination of the anion and cation concentrations in the urban wastewater sample have been reported in our recent work (Ye et al., 2020). The PS concentration was obtained following the colorimetric method described by Liang et al. (2008), using a Shimadzu 1800 UV/vis spectrophotometer set at λ = 484 nm. The Fe^{2+} concentration was determined from the red complex formed with 1,10-phenanthroline using the same spectrophotometer, set at λ = 510 nm. The total iron content of the solutions was obtained using ascorbic acid to reduce Fe^{3+} to Fe^{2+}.

The aliquots collected from treated solutions were diluted with methanol to stop the degradation process and filtered with 0.45 μm PTFE Whatman filters to determine the BPA concentration by reversed-phase HPLC. This analysis was carried out by injecting 10 μL into a Waters system composed of a 600 liquid chromatograph coupled to a 996 photodiode array detector set at λ = 290 nm. The chromatograph was fitted with a BDS Hypersil C18, 250 mm × 4.6 mm, column at 25 ºC, and a 40:60 (v/v) acetonitrile/water (KH_2PO_4 10 mM, pH 3) mixture was eluted as mobile phase at 1.0 mL min^{-1}. In the chromatograms, a well-defined peak for BPA was displayed at retention time (t_r) of 4.2 min.

For monitoring the solution mineralization, the above filtered aliquots were immediately injected into a Shimadzu VCSN TOC analyzer. Average values from experiments made in duplicate are discussed in this work, and figures show the error bar related to the 95% confidence interval.

Taking into account that the overall mineralization for BPA can be written as shown in Eq. (13), involving a number of consumed electrons (*n*) of 72 (Burgos-Castillo et al., 2018):

$$C_{15}H_{16}O_2 + 28H_2O \rightarrow 15CO_2 + 72H^+ + 72e^- \quad (13)$$

and based on the experimental TOC abatement ($\triangle(TOC)_{exp}$, in mg L^{-1}) for a given test at current *I* (in A) and time *t* (in h), the mineralization current efficiency (MCE, in %) was estimated as follows (dos Santos et al., 2018b, 2018c):

$$\%\ MCE = \frac{n\ F\ V \triangle(TOC)_{exp}}{4.32\times10^7\ m\ I\ t}\ 100 \quad (14)$$

where *F* denotes the Faraday constant, *V* is the solution volume (in L), *m* is the number of carbon atoms of the BPA molecule (= 15) and a constant has been included to convert units. The specific energy consumption per unit TOC mass (EC_{TOC}, in kWh (kg TOC)$^{-1}$) was calculated as suggested by Steter et al. (2016).

The primary by-products of BPA degradation were identified by electrolyzing a BPA solution in an IrO_2/carbon-felt cell. The resulting organics were extracted with CH_2Cl_2, and the resulting volume was dried over anhydrous Na_2SO_4, filtered and reduced to about 1 mL in order to be analyzed by GC-MS. To do this, the same equipment and procedure described in earlier work was utilized (Steter et al., 2016). The chromatographic separation was made with a polar HP INNOWax 0.25 μm, 30 m × 0.25 mm, column and the compounds were identified by comparing their mass spectra with those listed in the NIST05 MS database.

3. Results and discussion

3.1. Treatment of BPA solutions using PS, Fe^{2+} and a carbon-felt cathode

Some blank assays were performed with solutions that contained 0.140 mM BPA (25 mg L^{-1} TOC) in 0.050 M Na_2SO_4 medium at pH 3.0 and 35 ºC. An IrO_2/carbon-felt cell was employed, giving rise to the EO process at *I* = 100 mA. The initial pH 3.0 was selected because

it is optimal for oxidation processes involving Fe^{2+} (Yan et al., 2019). In these trials, no significant pH changes were found over time. Fig. 1a shows a very poor and similar degradation rate when the solutions were treated by EO in the absence of PS and Fe^{2+} and the presence of either 5.0 mM PS or 0.20 mM Fe^{2+}. Table 1 shows that 19-22% BPA removal was achieved in the three cases after 60 min of electrolysis. This allows inferring that the main oxidant was the weak $IrO_2(^{\bullet}OH)$ species formed from reaction (7), whereas PS yielded much lower amounts of oxidizing agents, i.e., the rate of reactions (8) and (10) was rather insignificant. Furthermore, it is clear that the contribution of $^{\bullet}OH$ potentially formed from Fenton's reaction with cathodically generated H_2O_2 can be disregarded, as expected from the absence of O_2 sparging during the experiments. In contrast, a very rapid BPA decay can be observed as a result of the electro/Fe^{2+}/PS treatment (Fig. 1a), attaining 98.4% abatement at the end of the treatment (see Table 1). This quicker degradation can be accounted for by the large production of $SO_4^{\bullet-}$ from activated PS via reaction (1), which can be partially transformed into homogeneous $^{\bullet}OH$ via reaction (4). In that process, the target molecule was then mainly oxidized by these radicals, playing $IrO_2(^{\bullet}OH)$ a relatively minor role.

The concentration decay in the above trials was analyzed in detail by simple kinetic equations. Fig. 1b depicts the good linear profiles obtained when a pseudo-first-order reaction was considered. This kind of behavior suggests the formation of a small but steady quantity of oxidizing species in each treatment. The pseudo-first-order rate constants (k_1) determined from such analysis are collected in Table 1, being always associated to excellent squared correlation coefficients (R^2) > 0.99. The k_1-values for the three mild EO processes were quite similar, varying between 0.0034 and 0.0040 min^{-1}, which confirms that the oxidation was caused mainly by $IrO_2(^{\bullet}OH)$. Nevertheless, the k_1-value obtained in the electro/Fe^{2+}/PS treatment was 26.9-31.6-fold greater, as corresponded to the much greater reactivity of $SO_4^{\bullet-}$ and homogeneous $^{\bullet}OH$.

The mineralization of the same solutions was monitored by measuring their TOC removal. Fig. 1c presents the change of the normalized TOC decay with time during the above experiments. Since the mineralization process involves the overall destruction of all the intermediates, it is considerably slower than the degradation of the target pollutant (Burgos-Castillo et al., 2018). Thus, the three first EO processes yielded less than 8% TOC abatement at 60 min, whereas the electro/Fe^{2+}/PS one allowed reaching a larger mineralization of 61.8%. This means that in the latter process, $IrO_2(^{\bullet}OH)$, $SO_4^{\bullet-}$ and homogeneous $^{\bullet}OH$ not only reacted rapidly with BPA but also caused the gradual degradation of its oxidation products.

From these results, the MCE values were calculated from Eq. (14) and their time course is shown in Fig. 1d. Insignificant current efficiencies < 3% were found in the three mild EO treatments, in agreement with the scarce mineralization achieved (see Fig. 1c). Conversely, in the case of the electro/Fe^{2+}/PS process, the MCE values were much greater, although the efficiency dropped down progressively from 44.0% at 10 min to 21.6% at 60 min. This trend can be explained by the appearance of more recalcitrant products and the lower organic load as the electrolysis proceeded (Thiam et al., 2015; Steter et al., 2016).

Another parameter of interest, the energy consumption, was determined as well. The data of Table 1 evidence a cell voltage (E_{cell}) of 5.1 V in all these trials, representing a consumption of 3.92 kWh m^{-3}. To better characterize the performance of the treatments, the EC_{TOC} value at 60 min was calculated from Eq. (15). The lowest EC_{TOC} (253.9 kWh (kg TOC)$^{-1}$) arouse from the electro/Fe^{2+}/PS process.

3.2. Effect of the anode and cathode material in the electro/Fe^{2+}/PS process

Once demonstrated the effectiveness of generated $SO_4^{\bullet-}$ and $^{\bullet}OH$ to remove BPA upon application of the electro/Fe^{2+}/PS process, the influence of the M($^{\bullet}OH$) nature was assessed by replacing the anode material (M). The electrolysis of the 0.140 mM BPA solution in acidic sulfate medium was made in the presence of 5.0 mM PS and 0.20 mM Fe^{2+} at 100 mA, using a

non-active BDD or an active Pt anode, the latter with an expected oxidation power similar to that of the IrO_2-based anode (Panizza and Cerisola, 2009; Martínez-Huitle et al., 2015). In Fig. 2a, the quicker BPA degradation using Pt as compared to IrO_2 is evidenced, which is further enhanced with BDD. Total removal was achieved after 40 and 50 min using BDD and Pt, respectively, whereas the use of the DSA led to 98.4% decay at 60 min (see Table 1). This agrees with the much higher oxidation power of generated BDD($^{\bullet}$OH), when compared to Pt($^{\bullet}$OH) and IrO_2($^{\bullet}$OH) (Steter et al., 2016). The different oxidation ability of these electrodes can also be observed from the good pseudo-first-order kinetic analysis of the concentration decays presented in the inset panel of Fig. 2a. Based on the data of Table 1, the k_1-value increased 1.50 and 1.69 times using Pt and BDD, respectively, confirming the superiority of the BDD anode.

The positive effect of replacing the IrO_2-based anode by Pt or BDD for improving the BPA removal was corroborated when the TOC decay was determined (data not shown). After 60 min of electrolysis, 63.1% and 70.7% mineralization were achieved using those anodes, related to MCE values of 22.0% and 24.7%, respectively, becoming better than 61.8% mineralization and 21.6% MCE determined for the DSA. However, the EC_{TOC} values (301.8 kWh (kg TOC)$^{-1}$ with Pt and 365.6 kWh (kg TOC)$^{-1}$ with BDD) were high as compared to 253.9 kWh (kg TOC)$^{-1}$ calculated in the IrO_2/carbon-felt cell, as result of the higher E_{cell} of their cells (see Table 1). Therefore, although the BDD anode yielded a quicker degradation and mineralization, the IrO_2-based anode turned out to be more cost-effective. This was the best anode to run the electro/Fe^{2+}/PS treatment because of the minor influence of the physisorbed M($^{\bullet}$OH) originated at the anode in this type of system, being the generated $SO_4^{\bullet-}$ the predominant oxidant.

On the other hand, several authors have proposed the use of SS as the cathode for PS activation promoted by an effective Fe^{2+} regeneration via reaction (11) (Wu et al., 2012). To clarify if the 3D carbon-felt cathode can provide a better oxidation ability to the electrolytic

system, the effect of the cathode over the electro/Fe^{2+}/PS process performance was examined. Fig. 2b shows that, in the absence of current supply, the BPA decay caused by a mixture of 5.0 mM PS + 0.20 mM Fe^{2+} was only 14.2% at 60 min, suggesting that the extent of reaction (1) between the two species to form $SO_4^{\bullet-}$ was very limited, probably due to the rapid decay of Fe^{2+} concentration. This assumption was confirmed by analyzing the change of PS and iron ions content during this treatment, which is depicted in Fig. 2c and 3a, respectively. As can be seen in Fig. 2c, the PS concentration dropped down rapidly for 30 min (10.6% decay), and more slowly up to 60 min (14.5% decay at that time), accounting for a total loss of 0.70 mM. In agreement, Fig. 3a makes in evidence the overall oxidation of Fe^{2+} to Fe^{3+} in about 30-40 min, thus justifying the little effectiveness of PS activation to destroy the target molecule.

Fig. 2b highlights a positive effect on BPA degradation when SS was used as the cathode connected to the IrO_2-based anode. The BPA disappearance reached a 31.0% at the end of that electro/Fe^{2+}/PS treatment. This enhancement, as compared to the previous trial without current supply, can be ascribed to the Fe^{2+} regeneration from reaction (11) at the SS surface, originating a larger content of oxidants $SO_4^{\bullet-}$ and homogeneous $^{\bullet}OH$ from reactions (1) and (4). Accordingly, a faster PS destruction can be observed in Fig. 2c, attaining a 28.7% (1.43 mM). Worth noting, this effect was much more remarkable using the 3D carbon-felt cathode, since 98.4% of the initial compound was removed (see Fig. 2b). for this experiment, Fig. 2c shows a drastic decay of 92.7% (4.63 mM) of the initial PS concentration (5.0 mM), which explains the rapid degradation and mineralization found for the BPA solution. The quicker PS disappearance with carbon felt confirms its ability to electroregenerate Fe^{2+}. This phenomenon was confirmed by measuring the high Fe^{2+} content remaining in the bulk at the end of the electrolysis, as can be seen in Fig. 3a. This ion decayed from an initial concentration of 0.20 mM to a minimal of 0.085 mM at 30 min, whereupon it gradually increased up to 0.126 mM. Fe^{2+} was oxidized to Fe^{3+} via reactions (1), (2) and (12), but its continuous cathodic regeneration via reaction (11)

prevailed. Based on these results, it is evident that the 3D carbon-felt cathode outperforms the SS one to regenerate Fe^{2+}, and its combination with a relatively cheap IrO_2-based anode gives rise to the most promising electro/Fe^{2+}/PS process.

3.3. Identification of oxidizing agents

The nature of the oxidizing agents produced in the electro/Fe^{2+}/PS treatment of acidic BPA solutions was ascertained in two independent trials by adding *tert*-butanol or methanol as scavengers to the IrO_2/carbon-felt cell containing an acidic BPA solution with Na_2SO_4, PS and Fe^{2+}. The former is known to react selectively with homogeneous and heterogenous hydroxyl radical, whereas methanol reacts with both, hydroxyl radicals and sulfate radical anion.

Fig. 3b highlights that the BPA concentration was reduced by 62.3% when *tert*-butanol was present in the solution, whereas after methanol addition, it only decreased by 11.0%. Considering that in the absence of scavengers, this content decayed by 98.4% (see also Table 1), whereas in the simple EO process without PS and Fe^{2+}, $IrO_2(^{\bullet}OH)$ led to 21.6% abatement, one can infer, as a first approach, that the $SO_4^{\bullet-}$ and homogeneous $^{\bullet}OH$ contributed to 51.3% and 14.5% of the overall BPA degradation, respectively. This means that the amount of generated oxidizing agents increased in the sequence: homogeneous $^{\bullet}OH < IrO_2(^{\bullet}OH) < SO_4^{\bullet-}$. The main oxidant in this process is $SO_4^{\bullet-}$ produced from reaction (1) and, for this reason, the Fe^{2+} regeneration at the cathode becomes crucial to achieve a fast pollutant removal. This radical can also be a source of $^{\bullet}OH$ from reaction (4), contributing to the attack onto the organics. However, parasitic reactions like (2) and (6) can limit the decontamination that is finally achieved, thus being necessary to optimize the operation conditions.

3.4. Effect of operation parameters on BPA degradation using an IrO_2/carbon-felt cell

The effect of key variables, namely PS, Fe^{2+} and BPA concentrations and applied *I*, on the performance of the electro/Fe^{2+}/PS process at pH 3.0 was examined. The assays lasted for 60

min as maximal, since it was found that practically all PS was consumed at that time (see Fig. 2c). The normalized concentration-time plots obtained in these runs are shown in Fig. 4a-d. The excellent linear correlations found in all cases assuming a pseudo-first-order kinetics are presented in the inset panels, whereas the k_1-values obtained, alongside the R^2 (usually > 0.99), are summarized in Table 1.

The influence of PS content between 1.0 and 10.0 mM was studied by electrolyzing a 0.140 mM BPA solution with 0.20 mM Fe^{2+} at 100 mA. Fig. 4a highlights the gradually greater concentration abatement as the PS content became higher. The lowest PS concentration only yielded a 60.0% degradation (see Table 1), whereas overall removal was achieved at 30 min using 10.0 mM PS. Table 1 also shows that the rise of k_1-value within the selected concentration range was roughly linear. This suggests that the degradation process was governed by reaction (1), which originates the main oxidant $SO_4^{\bullet-}$ and, concurrently, $^{\bullet}OH$ via reaction (4). These two species acted on the initial pollutant and its oxidation products.

The effect of the Fe^{2+} concentration within the range of 0.05-0.50 mM when treating 0.140 mM BPA solutions with 5.0 mM PS at 100 mA was less clear. A gradual increase in the degradation rate of the pollutant as the Fe^{2+} content was risen can be observed in Fig. 4b. At 0.05 mM Fe^{2+}, 85.5% of the target molecule disappeared at 60 min, whereas total BPA decay was already reached at 40 min using 0.50 mM (see Table 1). This tendency is expected if the larger presence of Fe^{2+} regenerated from reaction (11) accelerates the generation of oxidizing agents from reaction (1). However, a 4.5-fold increase of the k_1-value was associated to a tenfold rise in Fe^{2+} concentration (see Table 1), suggesting a progressive drop of the relative proportion of regenerated Fe^{2+} from reaction (1). Here, it can be presumed that parasitic reactions (2) and (12) that consume the Fe^{2+} are gradually favored as its content increases. Since an excessive amount of this ion is detrimental, owing to the need of iron hydroxide sludge

management once the treated effluent must be neutralized before discharge, 0.20 mM Fe^{2+} was considered an optimal for BPA removal.

For solutions with 5.0 mM and 0.20 mM Fe^{2+} treated at 100 mA, the increase of BPA concentration from 0.070 to 0.280 mM decelerated its degradation, as can be observed in Fig. 4c. Total disappearance was reached at 30 min when treating the most diluted solution. The k_1-value underwent a drastic reduction from 0.1941 min^{-1} (see Table 1). A deeper analysis of the data of Fig. 4c allows deducing an upgrading of the oxidation power of the electrolytic system as the BPA concentration became higher. For example, at 30 min, when the 0.070 mM BPA solution was completely degraded, concentrations removed attained 0.134 and 0.196 mM when starting with 0.140 and 0.280 mM, respectively. The effective destruction of this compound indicates the attack of greater amounts of oxidizing agents, thanks to the decrease in rate of their parasitic phenomena like reaction (2).

The effect of the supplied current was analyzed by applying from 25 to 200 mA to a cell containing a 0.140 mM BPA solution with 5.0 mM PS and 0.20 mM Fe^{2+}. Fig. 4d depicts an enhancement of the degradation rate with increasing *I* and thus, the initial pollutant was completely abated in 30 min at 200 mA whereas it attained a 97.7% reduction at 25 mA. This behavior was also evidenced from the increased k_1-value, from 0.0634 to 0.1607 min^{-1}, within the *I* range (see Table 1). This represents a 2.5-fold rise of k_1 related to an 8-fold growth of *I*, resulting from the gradually greater consumption of *I* in parasitic reactions, including the conversion of a larger proportion of $IrO_2(^{\bullet}OH)$ into O_2 gas at the anode (Panizza and Cerisola, 2009). Despite this, the oxidation ability of the system was actually upgraded, since greater quantities of $IrO_2(^{\bullet}OH)$ and Fe^{2+} were formed via reactions (7) and (11), respectively, favoring a larger production of $SO_4^{\bullet-}$ and homogeneous $^{\bullet}OH$ from reactions (1) and (4). The value of 100 mA can be considered as optimal, since practically all PS was consumed at 60 min (see Fig. 2c). Lower *I* values yielded a similar degradation at that time (see Table 1), being expected

that they consumed less PS and hence, that the final mineralization was smaller. However, the energy consumption could also be smaller due to the lower E_{cell} (see Table 1).

3.5. Identification of primary by-products and proposed degradation route for BPA

The primary by-products originated from the electro/Fe^{2+}/PS treatment of a solution with 0.140 mM BPA, 0.050 M Na_2SO_4, 5.0 mM PS and 0.20 mM Fe^{2+} at pH 3.0, 35 ºC and 100 mA after 15 min were identified by GC-MS. Table SM-1 summarizes the characteristics of BPA (compound **1**), two dehydroxylated benzene derivatives (compounds **2** and **3**) and three hydroxylated benzene by-products (compounds **4**-**6**). It has been documented that in the presence of activated PS, BPA can be dehydroxylated to yield 4,4'-(propane-2,2-diyl)dibenzene. The subsequent cleavage of this molecule and BPA at the the vulnerable C-C bond between the two benzene rings generates some monobenzenes (Lin et al., 2017; Ma et al., 2018). This behavior has been confirmed in our system, clearly evidencing the existence of two parallel initial degradation routes for BPA, as proposed in Fig. 5. The first one involves the attack of $SO_4^{\bullet-}$, causing the dehydroxylation of **1** followed by the cleavage of the central C-C bond to yield **2**, which is subsequently oxidized to **3**. The formation of **2** and **3** using activated PS has been reported by Lin et al. (2017), whereas only **3** has been detected by Ma et al. (2018). The second route corresponds to the attack of $^{\bullet}OH$ and produces the cleavage of **1** to generate a mixture of **4** and **5**. Further hydroxylation of **5** leads to **6**. . Compound **4** can also be formed from hydroxylation of **2**. The production of these three hydroxylated benzenes has been described by Ding et al. (2020) by means of EO with activated PS using a BDD anode. The two latter benzenes were found by Burgos-Castillo et al. (2018) using several EAOPs that generated $^{\bullet}OH$ on site.

3.6. Treatment of BPA spiked into urban wastewater

The assessment of the electro/Fe^{2+}/PS process performance was extended to urban wastewater. This matrix contains two components such as Cl^- and natural organic (NOM) due to the presence of humic, fulvic and tannic acids, which can affect the oxidation power of the electrochemical system. The assays were made by spiking 0.140 mM BPA into urban wastewater, whose pH was adjusted to 3.0 in order to compare with the trials made in sulfate medium. The electrolyses were made in an IrO_2/carbon-felt cell at 100 mA for 60 min.

Fig. 6a shows that, under EO conditions, the pollutant concentration decayed gradually to attain a removal of 45.1%. This value was much greater than 21.6% obtained in the analogous treatment in sulfate medium (see Table 1). Such an enhancement can be related to the production of active chlorine (HOCl) from the anodic oxidation of Cl^- according to reactions (15) and (16) (Thiam et al., 2015). HOCl competes with $IrO_2(^{\bullet}OH)$ to attack BPA.

$$2Cl^- \rightarrow Cl_2 + 2e^- \quad (15)$$

$$Cl_2 + H_2O \rightarrow HOCl + Cl^- + H^+ \quad (16)$$

When 5.0 mM PS was added to the above wastewater sample, a quicker concentration reduction was found (78.9%, see Fig. 6a), being also clearly greater than 18.6% determined in the homologous treatment in sulfate medium (see Table 1). This behavior suggests the direct attack of PS on NOM, producing additional amounts of $SO_4^{\bullet-}$ via reaction (3). In the presence of Cl^-, $SO_4^{\bullet-}$ can produce the strong oxidant $^{\bullet}OH$ according to reactions (17)-(19) (Lutze at al., 2015).

$$SO_4^{\bullet-} + Cl^- \rightarrow SO_4^{2-} + Cl^{\bullet} \quad (17)$$

$$Cl^{\bullet} + H_2O \rightarrow HOCl^{\bullet-} + H^+ \quad (18)$$

$$HOCl^{\bullet-} \leftrightarrows {}^{\bullet}OH + Cl^- \quad (19)$$

In the electro/Fe^{2+}/PS treatment with 5.0 mM PS and 0.20 mM Fe^{2+}, the BPA content was completely abated in 40 min (see Fig. 6a), outperforming the trial made in sulfate medium (see

Fig. 1a). This enhancement can then be ascribed to the simultaneous oxidation by $IrO_2(^{\bullet}OH)$, $SO_4^{\bullet-}$, homogeneous $^{\bullet}OH$ and HOCl. Based on the large $SO_4^{\bullet-}$ production from reaction (1), a large $^{\bullet}OH$ generation is expected from reactions (17)-(19).

The good agreement of the above content decays with a pseudo-first-order kinetics is presented in Fig. 6b. In the electro/Fe^{2+}/PS treatment, the k_1-value in urban wastewater was 1.5-fold higher than that determined in sulfate medium (see Table 1), confirming the occurrence of greater amounts of oxidizing agents in the actual wastewater. As a result, the contaminated urban wastewater with 36.8 mg L^{-1} TOC was more largely mineralized. The mineralization attained 69.3%, which partly involved the degradation of NOM. The EC_{TOC} in this matrix was higher as compared to the sulfate medium (289.5 kWh (kg TOC)$^{-1}$) due to the lower conductivity.

4. Conclusions

The electro/Fe^{2+}/PS process with an IrO_2/carbon-felt cell is very effective for the degradation of acidic BPA solutions. This technology outperformed the EO due to the large production of $SO_4^{\bullet-}$, which was more abundant than homogeneous $^{\bullet}OH$. The combined action of these oxidants and $IrO_2(^{\bullet}OH)$ led to 98.4% degradation with 61.8% TOC removal after 60 min of electrolysis using 5.0 mM PS and 0.20 mM Fe^{2+} at 100 mA. Almost all PS was consumed during the treatment. BDD anode performed better than Pt and IrO_2, but it was led cost-effective. The 3D carbon-felt cathode became much more efficient than SS for Fe^{2+} regeneration. It can thus be concluded that the IrO_2/carbon-felt cell is the most adequate to run the electro/Fe^{2+}/PS process. All the concentration decays agreed with a pseudo-first-order kinetics. The oxidation power of the electrolytic system was enhanced at higher BPA content and applied *I*. Two dehydroxylated benzene derivatives were formed upon $SO_4^{\bullet-}$ attack on BPA, whereas three hydroxylated benzene by-products resulted from the action of $^{\bullet}OH$. The

degradation and the mineralization in urban wastewater were much quicker than in sulfate medium due to the additional generation of HClO. Our results suggest the attack of PS on NOM, producing extra $SO_4^{\bullet-}$.

Acknowledgements

The authors thank the funding from projects CTQ2016-78616-R (AEI/FEDER, EU) and PID2019-109291RB-I00 (AEI, Spain), as well as from the Coordenação de Aperfeiçoamento de Pessoal de Nível Superior - Brazil (CAPES) - Finance Code 001. A.J. dos Santos is grateful for the economic support from CAPES (Brazil) through the program "Pesquisa Pós-doutoral no Exterior" number 88881.172332/2018-01.

References

Akbari, S. Ghanbari, F., Moradi, M., 2016. Bisphenol A degradation in aqueous solutions by electrogenerated ferrous ion activated ozone, hydrogen peroxide and persulfate: applying low current density for oxidation mechanism. Chem. Eng. J. 294, 298-307.

Armstrong, D.A., Huie, R.E., Lymar, S., Koppenol, W.H., Merényi, G., Neta, P., Stanbury, D.M., Steenken, S., Wardman, P., 2015. Standard electrode potentials involving radicals in aqueous solution: inorganic radicals (IUPAC Technical Report). Pure Appl. Chem. 87, 1139-1150.

Bhatnagar, A., Anastopoulos, I., 2017. Adsorptive removal of bisphenol A (BPA) from aqueous solution: A review. Chemosphere 168, 885-902.

Brillas, E., 2020. A review on the photoelectro-Fenton process as efficient electrochemical advanced oxidation for wastewater remediation. Treatment with UV light, sunlight, and coupling with conventional and other photo-assisted advanced technologies. Chemosphere 250, 126198

Burgos-Castillo, R.C., Sirés, I., Sillanpää, M., Brillas, E., 2018. Application of electrochemical advanced oxidation to bisphenol A degradation in water. Effect of sulfate and chloride ions. Chemosphere 194, 812-820.

Careghini, A., Mastorgio, A.F., Saponaro, S., Sezenna, E., 2015. Bisphenol A, nonylphenols, benzophenones, and benzotriazoles in soils, groundwater, surface water, sediments, and food: A review. Environ. Sci. Pollut. Res. 22, 5711-5741.

Chmayssem, A., Taha, S., Hauchard, D., 2017. Scaled-up electrochemical reactor with a fixed bed three-dimensional cathode for electro-Fenton process: application to the treatment of bisphenol A. Electrochim. Acta 225, 435-442.

Corrales, J., Kristofco, L.A., Steele, W.B., Yates, B.S., Breed, C.S., Williams, E.S., Brooks, B.W., 2015. Global assessment of bisphenol A in the environment: Review and analysis of its occurrence and bioaccumulation. Dose Response 13, 1559325815598308.

Cui, Y.-H., Li, X.-Y., Chen, G., 2009. Electrochemical degradation of bisphenol A on different anodes. Water Res. 43, 1968-1976.

Devi, P., Das, U., Dalai, A.K., 2016. In-situ chemical oxidation: principle and applications of peroxide and persulfate treatments in wastewater systems. Sci. Total Environ. 571, 643-657.

Ding, J., Bu, L., Zhao, Q., Kabutey, F.T., Wei, L., Dionysiou, D.D., 2020. Electrochemical activation of persulfate on BDD and DSA anodes: electrolyte influence, kinetics and mechanisms in the degradation of bisphenol A. J. Hazard. Mater. 121789.

Dong, Z., Zhang, Q., Chen, B.-Y., Hong, J., 2019. Oxidation of bisphenol A by persulfate via Fe_3O_4-α-MnO_2 nanoflower-like catalyst: mechanism and efficiency. Chem. Eng. J. 357, 337-347.

dos Santos, A.J., de Araújo Costa, E.C.T., da Silva, D.R., Garcia-Segura, S., Martínez-Huitle, C.A., 2016. Influence of the water hardness on the performance of electro-Fenton

approach: decolorization and mineralization of Eriochrome Black T. Electrochim. Acta 208, 156-163.

dos Santos, A.J., de Araújo Costa, E.C.T., da Silva, D.R., Garcia-Segura, S., Martínez-Huitle, C.A., 2018a. Electrochemical advanced oxidation processes as decentralized water treatment technologies to remediate domestic washing machine effluents. Environ. Sci. Pollut. Res. 25, 7002–7011.

dos Santos, A.J., Martínez-Huitle, C.A., Sirés, I., Brillas, E., 2018b. Use of Pt and BDD anodes in the electrochemical advanced oxidation of Ponceau SS diazo dye in acidic sulfate medium. ChemElectroChem 5, 685-693.

dos Santos, A.J., Sirés, I., Alves, A.P.M., Martínez-Huitle, C.A., Brillas, E., 2020. Vermiculite as heterogeneous catalyst in electrochemical Fenton-based processes: application to the oxidation of Ponceau SS dye. Chemosphere 240, 124838.

dos Santos, A.J., Sirés, I., Martínez-Huitle, C.A., Brillas, E., 2018c. Total mineralization of mixtures of Tartrazine, Ponceau SS and Direct Blue 71 azo dyes by solar photoelectro-Fenton in pre-pilot plant. Chemosphere 210, 1137-1144.

El-Ghenymy, A., Rodríguez, R.M., Brillas, E., Oturan, N., Oturan, M.A., 2014. Electro-Fenton degradation of the antibiotic sulfanilamide with Pt/carbon-felt and BDD/carbon-felt cells. Kinetics, reaction intermediates, and toxicity assessment. Environ. Sci. Pollut. Res. 21, 8368-8378.

Galia, A., Lanzalaco, S., Sabatino, M.A., Dispenza, C., Scialdone, O., Sirés, I., 2016. Crosslinking of poly(vinylpyrrolidone) activated by electrogenerated hydroxyl radicals: A first step towards a simple and cheap synthetic route of nanogel vectors. Electrochem. Commun. 62, 64-68.

Girit, B., Dursun, D., Olmez-Hanci, T., Arslan-Alaton, I., 2015. Treatment of aqueous bisphenol A using nano-sized zero-valent iron in the presence of hydrogen peroxide and persulfate oxidants. Water Sci. Technol. 71, 1859-1868.

Gözmen, B., Oturan, M.A., Oturan, N., Erbatur, O., 2003. Indirect electrochemical treatment of bisphenol A in water via electrochemically generated Fenton's reagent. Environ. Sci. Technol. 37, 3716-3723.

Jiang, X., Wu, Y., Wang, P., Li, H., Dong, W., 2013. Degradation of bisphenol A in aqueous solution by persulfate activated with ferrous ion. Environ, Sci. Pollut. Res. 20, 4947-4953.

Kang, Y.-G., Vu, H.C., Le, T.T., Chang, Y.-S., 2018. Activation of persulfate by a novel Fe(II)-immobilized chitosan/alginate composite for bisphenol A degradation. Chem. Eng, J. 353, 736-745.

Khandarkhaeva, M., Batoeva, A., Sizykh, M., Aseev, D., Garkusheva, N., 2019. Photo-Fenton-like degradation of bisphenol A by persulfate and solar irradiation. J. Environ. Manage. 249, 109348.

Lanzalaco, S., Sirés, I., Galia, A., Sabatino, M.A., Dispenza, C., Scialdone, O., 2018. Facile crosslinking of poly(vinylpyrrolidone) by electro-oxidation with IrO_2-based anode under potentiostatic conditions. J. Appl. Electrochem. 48, 1343-1352.

Li, H., Long, Y., Wang, Y., Zhu, C., Ni, J., 2016. Electrochemical degradation of bisphenol A in chloride electrolyte-Factor analysis and mechanisms study. Electrochim. Acta 222, 1144-1152.

Liang, C., Huang, C.-F., Mohanty, N., Kurakalva, R.M., 2008. A rapid spectrophotometric determination of persulfate anion in ISCO. Chemosphere 73, 1540-1543.

Lin, H., Wu, J., Zhang, H., 2013. Degradation of bisphenol A in aqueous solution by a novel electro/Fe^{3+}/peroxydisulfate process. Sep. Purif. Technol. 117, 18-23.

Lin, K.-Y.A., Zhang, Z.-Y., 2017. Degradation of bisphenol A using peroxymonosulfate activated by one step prepared sulfur-doped carbon nitride as a metal-free heterogeneous catalyst. Chem. Eng. J. 313, 1320-1327.

Liu, J., Zhong, S., Song, Y., Wang, B., Zhang, F., 2018. Degradation of tetracycline hydrochloride by electro-activated persulfate oxidation. J. Electronal. Chem. 809, 74-79.

Luo, H., Li, C., Sun, X., Ding, B.B., 2017. Cathodic indirect oxidation of organic pollutant paired to anodic persulfate production. J. Electroanal. Chem. 792, 110-116.

Lutze, H.V., Kerlin, N., Schmidt, T.C., 2015. Sulfate radical-based water treatment in presence of chloride: Formation of chlorate, inter-conversion of sulfate radicals into hydroxyl radicals and influence of bicarbonate. Water Res. 72, 349-360.

Ma, W., Wang, N., Fan, Y. Tong, T., Han, X., Du, Y., 2018. Non-radical-dominated catalytic degradation of bisphenol A by ZIF-67 derived nitrogen-doped carbon nanotubes frameworks in the presence of peroxymonosulfate. Chem. Eng. J. 336, 721-731.

Martínez-Huitle, C.A., Rodrigo, M.A., Sirés, I., Scialdone, O., 2015. Single and coupled electrochemical processes and reactors for the abatement of organic water pollutants: A critical review. Chem. Rev. 115, 13362–13407.

Matuszczak, E., Komarowska, M.D., Debek, W., Hermanowicz, A., 2019. The impact of bisphenol A on fertility, reproductive system, and development: A review of the literature. Int. J. Endocrinol. 2019, 4068717.

Matzek, L.W., Carter, K.E., 2016. Activated persulfate for organic chemical degradation: a review. Chemosphere 151, 178-188.

Molkenthin, M., Olmez-Hanci, T., Jekel, M.R., Arslan-Alaton, I., 2013. Photo-Fenton-like treatment of BPA: Effect of UV light source and water matrix on toxicity and transformation products. Water Res. 47, 5052-5064.

Moreira, F.C., Boaventura, R.A.R., Brillas, E., Vilar, V.J.P., 2017. Electrochemical advanced oxidation processes: A review on their application to synthetic and real wastewaters. Appl. Catal. B: Environ. 202, 217-261.

Murugananthan, M., Yoshihara, S., Rakuma, T., Shirakashi, T., 2008. Mineralization of bisphenol A (BPA) by anodic oxidation with boron-doped diamond (BDD) electrode. J. Hazard. Mater. 154, 213-220.

Oturan, M.A., Aaron, J.J., 2014. Advanced oxidation processes in water/wastewater treatment: principles and applications. A review. Crit. Rev. Environ. Sci. Technol. 44, 2577-2641.

Panizza, M., Cerisola, G., 2009. Direct and mediated anodic oxidation of organic pollutants. Chem. Rev. 109, 6541-6569.

Petrie, B., Barden, R., Kasprzyk-Hordern, B., 2015. A review on emerging contaminants in wastewaters and the environment: Current knowledge, understudied areas and recommendations for future monitoring. Water Res. 72, 3-27.

Rochester, J.R., 2013. Bisphenol A and human health: A review of the literature. Reprod. Toxicol. 42, 132-155.

Romero, A., Santos, A., Vicente, F., González, C., 2010. Diuron abatement using activated persulphate: Effect of pH, Fe(II) and oxidant dosage. Chem. Eng. J. 162, 257-265.

Sirés, I., Garrido, J.A., Rodríguez, R.M., Brillas, E., Oturan, N., Oturan, M.A., 2007. Catalytic behavior of the Fe^{3+}/Fe^{2+} system in the electro-Fenton degradation of the antimicrobial chlorophene. Appl. Catal. B: Environ. 72, 382-394.

Steter, J.R., Brillas, E., Sirés, I., 2016. On the selection of the anode material for the electrochemical removal of methylparaben from different aqueous media. Electrochim. Acta 222, 1464-1474.

Thiam, A., Sirés, I., Garrido, J.A., Rodríguez, R.M., Brillas, 2015. Effect of anions on electrochemical degradation of azo dye Carmoisine (Acid Red 14) using a BDD anode and air-diffusion cathode. Sep. Purif. Technol. 140, 43-52.

Umar, M., Roddick, F., Fan, L., Aziz, H.A., 2013. Application of ozone for the removal of bisphenol A from water and wastewater - A review. Chemosphere 90, 2197-2207.

Wojnárovits, L., Takács, E., 2019. Rate constants of sulfate radical anion reactions with organic molecules: a review. Chemosphere 220, 1014-1032.

Wu, J., Wang, B., Cagnetta, G., Huang, J., Wang, Y., Deng, S., Yu, G., 2020. Nanoscale zero valent iron-activated persulfate coupled with Fenton oxidation process for typical pharmaceuticals and personal care products degradation. Sep. Purif. Technol. 239, 116534.

Wu, J., Zhang, H., Qiu, J., 2012. Degradation of Acid Orange 7 in aqueous solution by a novel electro/Fe^{2+}/peroxydisulfate process. J. Hazard. Mater. 215-216, 138-145.

Wu, P., Zhang, Y., Chen, Z., Duan, Y., Lai, Y., Fang, Q., Wang, F., Li, S., 2019. Performance of boron-doped graphene aerogel modified gas diffusion electrode for in-situ metal-free electrochemical advanced oxidation of bisphenol A. Appl. Catal. B: Environ. 255, 117784.

Xu, X., Zong, S., Chen, W., Liu, D., 2019. Comparative study of bisphenol A degradation via heterogeneously catalyzed H_2O_2 and persulfate: Reactivity, products, stability and mechanism. Chem. Eng. J. 369, 470-479.

Yan, S., Zhang, X., Zhang, H., 2019. Persulfate activation by Fe(III) with bioelectricity at acidic and near-neutral pH regimes: homogeneous versus heterogeneous mechanism. J. Hazard. Mater. 374, 92-100.

Yang, C.-W., 2015. Degradation of bisphenol A using electrochemical assistant Fe(II)-activated peroxydisulfate process. Water Sci. Eng. 8, 139-144.

Yang, Y., Guo, H., Zhang, Y., Deng, Q., Zhang, J., 2016. Degradation of bisphenol A using ozone/persulfate process: kinetics and mechanism. Water Air Soil Pollut. 227, 53.

Ye, Z., Schukraft, G.E.M., L'Hermitte, A., Xiong, Y., Brillas, E., Petit, C., Sirés, I., 2020. Mechanism and stability of an Fe-based 2D MOF during the photoelectro-Fenton treatment of organic micropollutants under UVA and visible light irradiation. Water Res. 184, 115986.

Figure captions

Fig. 1. (a) Normalized concentration decays, (b) pseudo-first-order kinetic analysis for each decay, (c) normalized TOC evolution and (d) mineralization current efficiency vs. electrolysis time during the treatment of 130 mL of solutions containing 0.140 mM BPA and 0.050 M Na_2SO_4 at pH 3.0, 100 mA and 35 ºC, using a stirred cell equipped with a 3 cm^2 IrO_2-based anode and a 30 cm^2 carbon-felt cathode. Method: (▽) EO, (■) EO with 5.0 mM PS, (▲) EO with 0.20 mM Fe^{2+} and (●) electro/Fe^{2+}/PS with 5.0 mM PS and 0.20 mM Fe^{2+}.

Fig. 2. (a) Effect of (▼) BDD, (▲) Pt and (●) IrO_2-based anode on the normalized BPA concentration abatement and its pseudo-first-order kinetics for the electro/Fe^{2+}/PS treatment of 130 mL of solutions containing 0.140 mM BPA, 0.050 M Na_2SO_4, 5.0 mM PS and 0.20 mM Fe^{2+} at pH 3.0, 100 mA and 35 ºC using a carbon-felt cathode. (b) Treatment of the same solution: (■) without current supply and (◆) with an IrO_2/SS cell. (c) Normalized PS concentration vs. time for the assays (■) without current supply and with the (◆) IrO_2/SS and (●) IrO_2/carbon-felt cell.

Fig. 3. (a) Time course of (◆,◇) Fe^{2+} and (▲,△) Fe^{3+} concentrations during the treatment of solutions of 130 mL containing 0.140 mM BPA, 0.050 M Na_2SO_4, 5.0 mM PS and 0.20 mM Fe^{2+} at pH 3.0 and 35 ºC. Method: (◇,△) Without current supply; (◆,▲) electro/Fe^{2+}/PS process with an IrO_2/carbon-felt cell at 100 mA. (b) Effect of scavengers on the normalized BPA concentration removal during the electro/Fe^{2+}/PS treatment of the solution described in (a): (▼) 500 mM methanol, (■) 500 mM *tert*-butanol and (●) without scavengers.

Fig. 4. Effect of experimental variables on normalized BPA concentration decay and its pseudo-first-order kinetics for the electro/Fe^{2+}/PS treatment of BPA in 0.050 M Na_2SO_4 medium at pH 3.0 and 35 ºC, using an IrO_2/carbon-felt cell. (a) [BPA]: 0.140 mM; [PS]: (◆) 2.0 mM, (●) 5.0 mM and (▲) 10.0 mM; [Fe^{2+}]: 0.20 mM; I = 100 mA. (b) [BPA]: 0.140 mM; [PS]: 5.0 mM;

[Fe^{2+}]: (▼) 0.05 mM, (◆) 0.10 mM, (●) 0.20 mM and (▲) 0.50 mM; *I* = 100 mA. (c) [BPA]: (▲) 0.070 mM, (●) 0.140 mM and (▼) 0.280 mM; [PS]: 5.0 mM; [Fe^{2+}]: 0.20 mM; *I* = 100 mA. (d) [BPA]: 0.140 mM; [PS]: 5.0 mM; [Fe^{2+}]: 0.20 mM; *I* = (◆) 25 mA, (■) 50 mA, (●) 100 mA and (▼) 200 mA.

Fig. 5. Initial stages of the degradation route of BPA in the electro/Fe^{2+}/PS treatment.

Fig. 6. (a) Normalized BPA concentration decays for the treatment of 130 mL of solutions containing BPA spiked at a concentration of 0.140 mM into urban wastewater at pH 3.0 and 35 ºC, using an IrO_2/carbon-felt cell at 100 mA. Method: (▲) EO, (◆) EO with 5.0 mM PS and (▼) electro/Fe^{2+}/PS with 5.0 mM PS and 0.20 mM Fe^{2+}. (b) Kinetic analysis assuming a pseudo-first-order reaction for BPA.

.

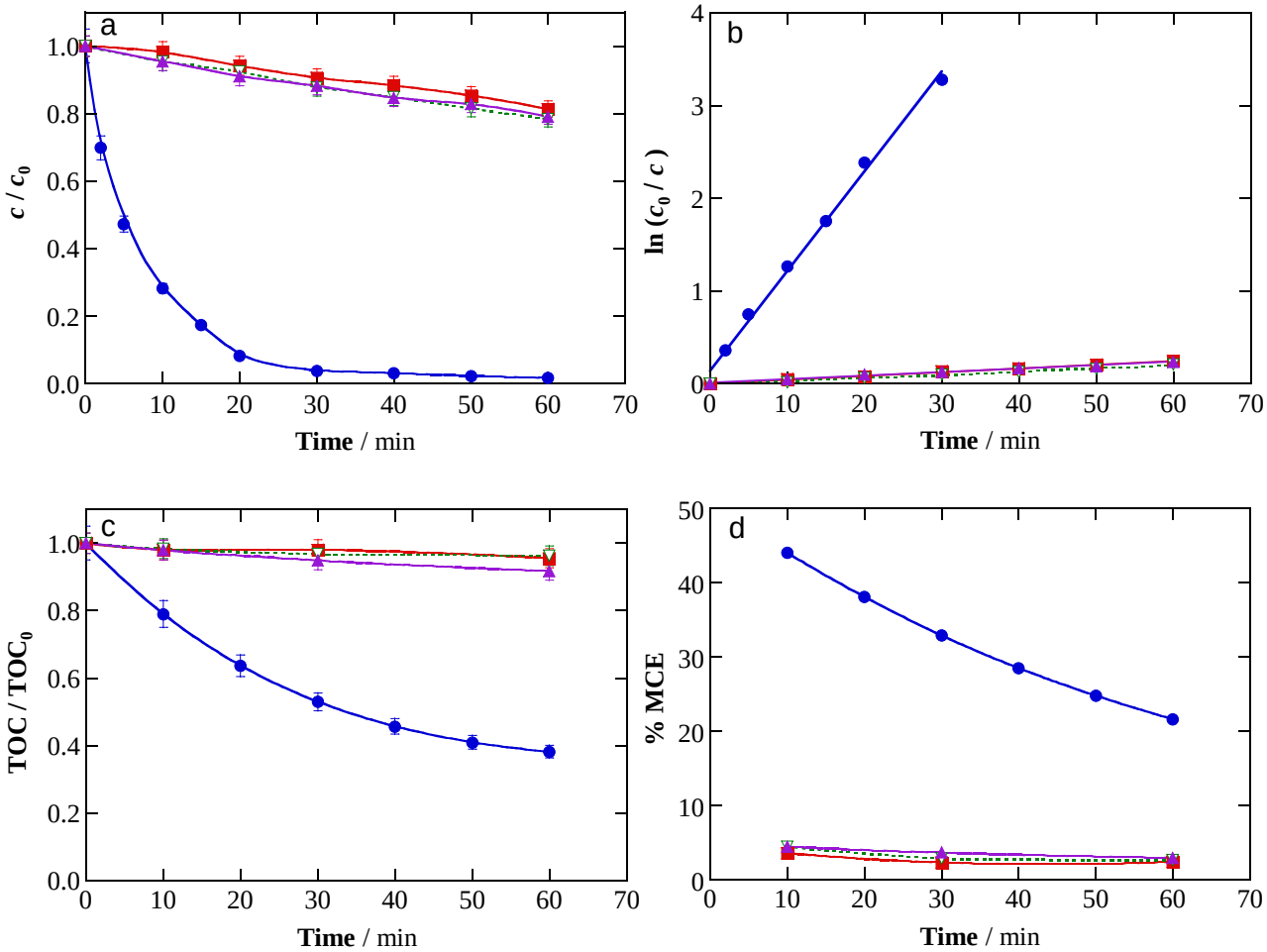
a
b
c
d
c / c0
ln (c0 / c)
TOC / TOC0
% MCE
Time / min
Time / min
Time / min
Time / min

Figure 1

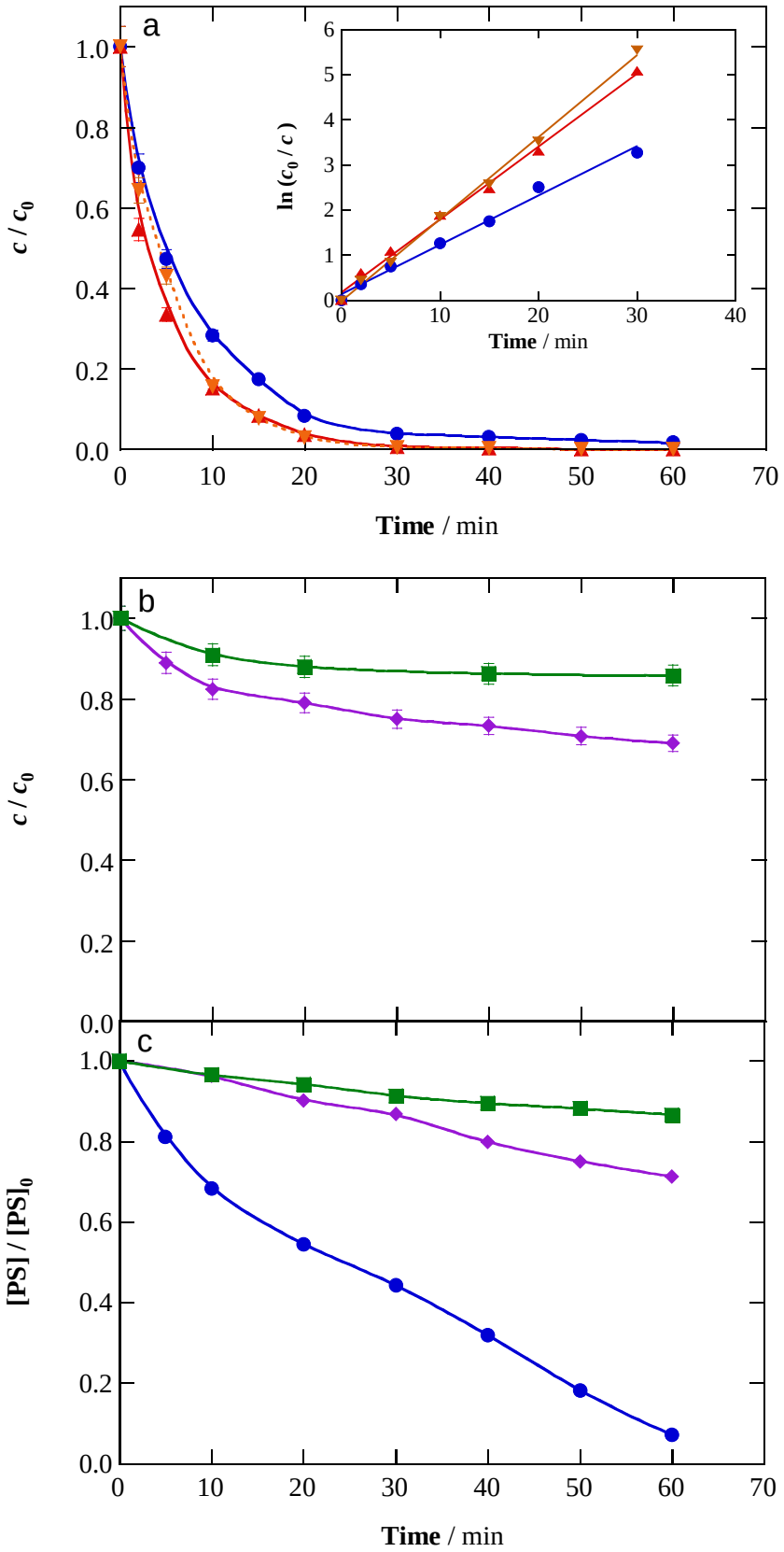

Figure 2

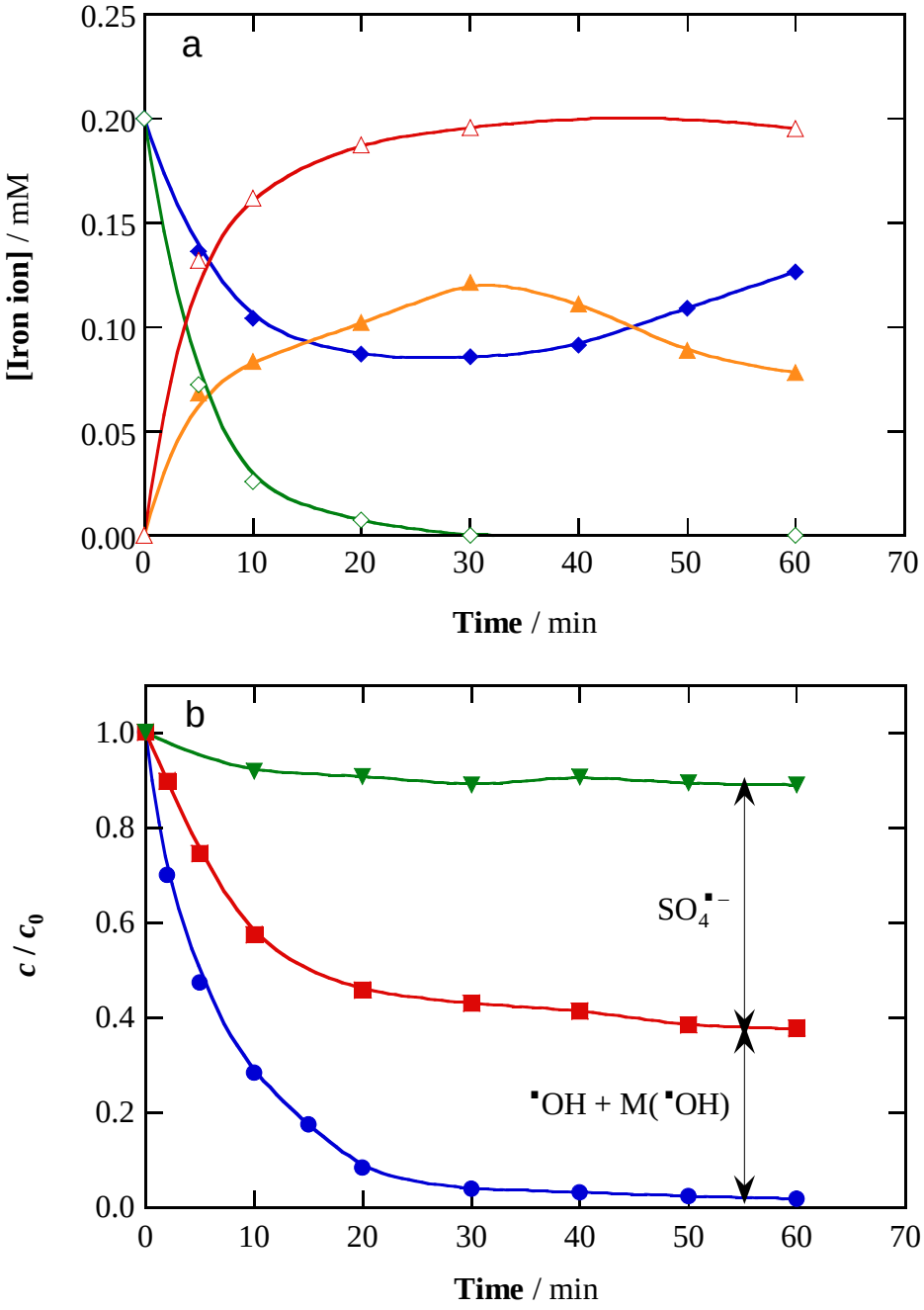
a
0.25
0.20
0.15
0.10
0.05
0.00
[Iron ion] / mM
0
10
20
30
40
50
60
70
Time / min
b
1.0
0.8
0.6
0.4
0.2
0.0
c / c0
SO4•−
•OH + M(•OH)
0
10
20
30
40
50
60
70
Time / min

Figure 3

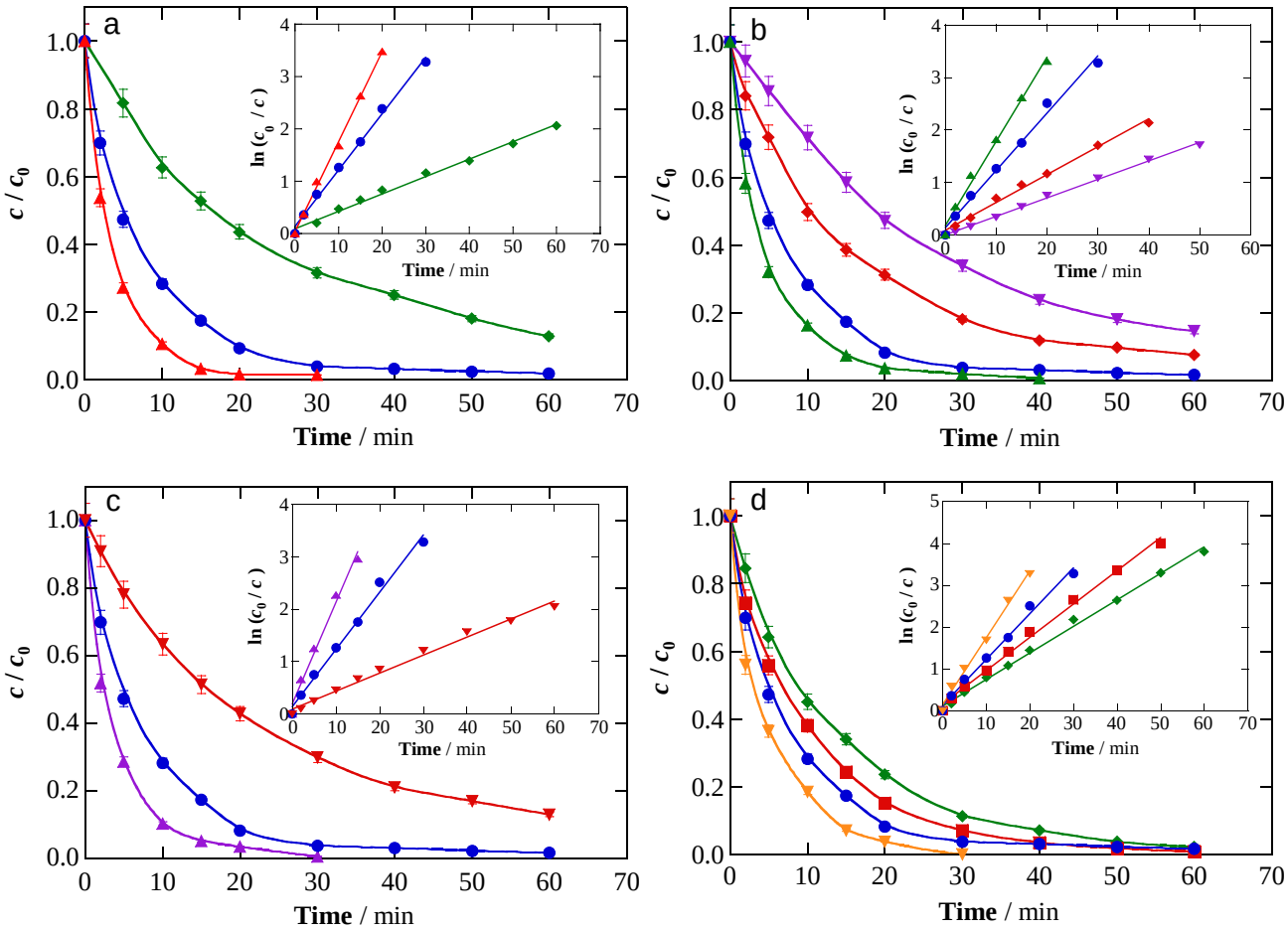

Figure 4

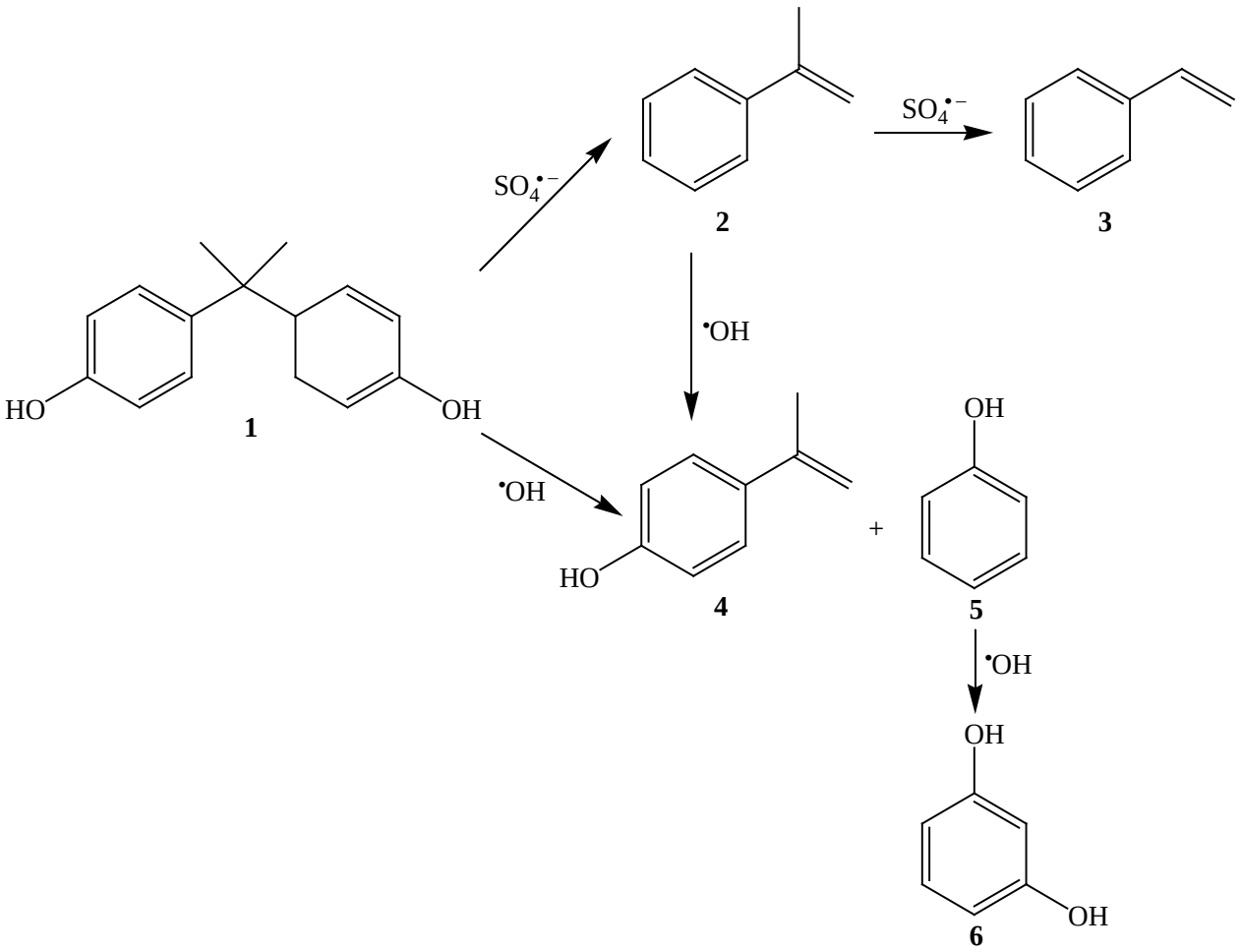

Figure 5

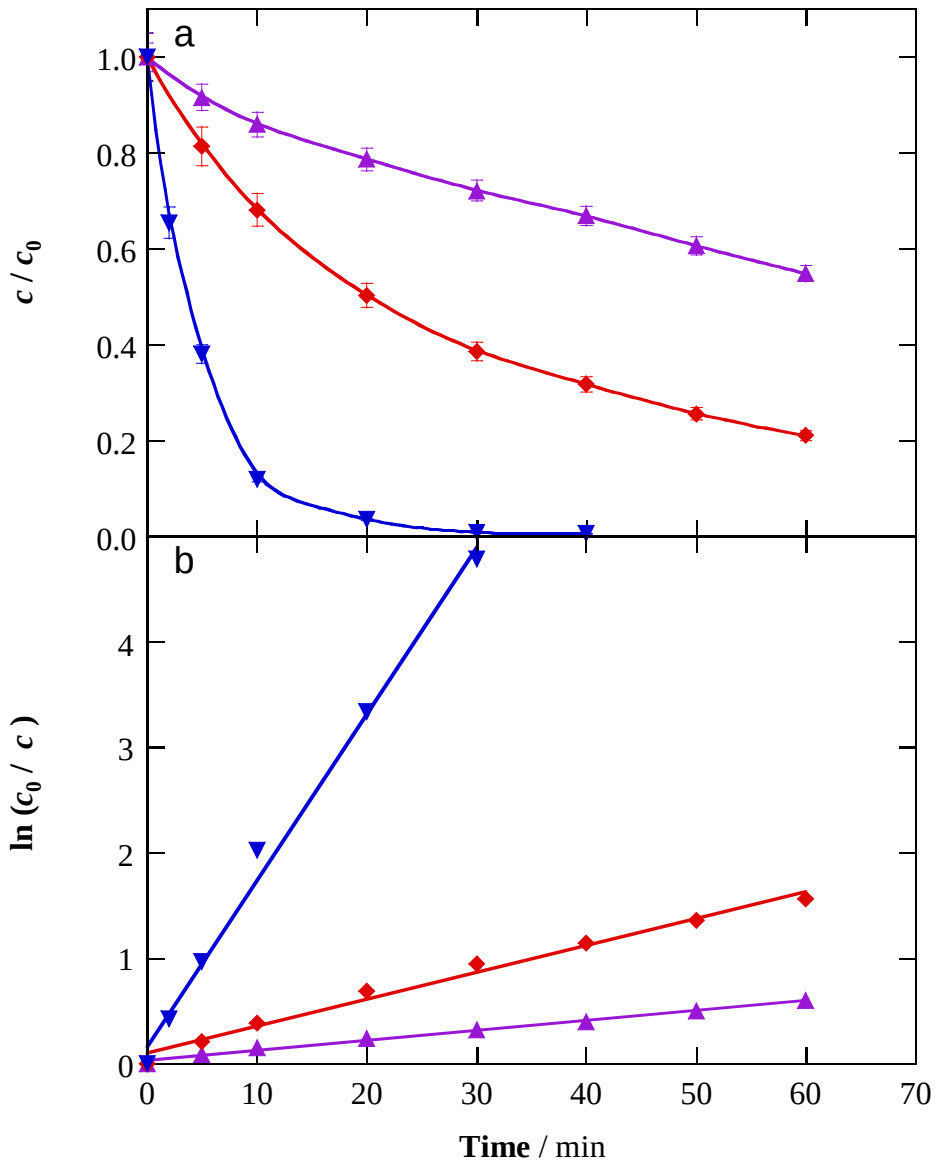

Figure 6

Table 1

Percentage of degradation and apparent rate constant for concentration decay. alongside the corresponding *R*-squared values, determined during the treatment of 130 mL of BPA solutions in 0.050 M Na_2SO_4 medium and urban wastewater at pH 3.0 and 35 ºC under different experimental conditions using a carbon-felt cathode.

Anode	[BPA] (mM)	[$Na_2S_2O_8$] (mM)	[Fe^{2+}] (mM)	*I* (mA)	E_{cell} (V)	% Degradation (time (min))	k_1 (min^{-1})	R^2
0.050 M Na_2SO_4								
BDD	0.140	5.0	0.20	100	8.4	100 (40)	0.1817	0.998
Pt	0.140	5.0	0.20	100	6.2	100 (50)	0.1617	0.995
IrO_2-based	0.140	-	-	100	5.1	21.6 (60)	0.0034	0.992
	0.140	5.0	-	100	5.1	18.7 (60)	0.0040	0.998
	0.140	-	0.20	100	5.1	20.9 (60)	0.0038	0.992
	0.070	5.0	0.20	100	5.1	100 (30)	0.1941	0.984
	0.140	1.0	0.20	100	5.1	60.0 (60)	0.0157	0.996
	0.140	2.0	0.20	100	5.1	87.3 (60)	0.0332	0.992
	0.140	5.0	0.05	100	5.1	85.5 (60)	0.0353	0.998
	0.140	5.0	0.10	100	5.1	92.4 (60)	0.0531	0.993
	0.140	5.0	0.20	25	3.1	97.7 (60)	0.0634	0.996
	0.140	5.0	0.20	50	4.3	98.6 (60)	0.0796	0.996
	0.140	5.0	0.20	100	5.1	98.4 (60)	0.1078	0.995
	0.140	5.0	0.20	200	8.2	100 (30)	0.1596	0.993
	0.140	5.0	0.50	100	5.1	100 (40)	0.1607	0.992
	0.140	10.0	0.20	100	5.1	100 (30)	0.1722	0.998
	0.280	5.0	0.20	100	5.1	87.0 (60)	0.0343	0.989
	0.560	5.0	0.20	100	5.1	57.1 (60)	0.0138	0.996
Urban wastewater								
IrO_2-based	0.140	-	-	100	9.6	45.1(60)	0.0094	0.993
	0.140	5.0	-	100	9.6	78.9 (60)	0.0255	0.986
	0.140	5.0	0.20	100	9.6	100 (40)	0.1576	0.993